Micro-Macro Transition for anisotropic, frictional granular packings

Stefan Luding [a,b]

[a] *Particle Technology, DelftChemTech, TUDelft,*
Julianalaan 136, 2628 BL Delft, The Netherlands
[b] *e-mail:* `s.luding@tnw.tudelft.nl`

Abstract

From the structure of a static granular solid, we derive the fabric, and the stiffness tensor in average over those pairs of interacting particles with contact within the averaging volume. Starting from a linear expansion of the interaction potential around static equilibrium, stress and elastic strain can be derived from the principles of virtual displacement and virtual stress-change, respectively. Our approach includes both normal and tangential forces separately, in a new modular formulation starting from single contacts.

The results are applied to a discrete particle simulation, and the findings include a relation between fabric and coordination number that is almost unaffected by the presence of friction, a different qualitative behavior of fabric and stiffness components, and only three independent entries to the stiffness matrix in its eigen-system. More general, anisotropy evolves directed against the direction of compression, and exponentially fast up to a certain maximal (limit) magnitude – a constitutive model for this behavior is proposed; in the critical state shear regime, the anisotropy is considerably smaller.

Key words: Anisotropy, Fabric tensor, Stiffness tensor, discrete element model

1 Introduction

One of todays great challenges in material science and physics is the macroscopic description of the material behavior of granular materials like sand, that are inhomogeneous, nonlinear, disordered, and anisotropic on a "microscopic" scale. This is due to the contact network of the static structure formed by the grains, but also due to the inhomogeneous stress distribution in granular assemblies and the corresponding force-networks. There are always large

fluctuations of contact forces and a reorganization of the network due to deformation can lead to a re-structuring of those. For example, when an initially isotropic contact network is deformed, the result is likely anisotropic in structure. We do not review the existing literature in this field here, rather we point the readers attention to the books by Herrmann et al. (1998); Vermeer et al. (2001); Kishino (2001) and some references by various groups (Chang and Ma, 1991; Babić, 1997; Bagi, 1999; Oda and Iwashita, 2000; Bardet and Vardoulakis, 2001; Suiker et al., 2001; Luding and Herrmann, 2001; Peters and Horner, 2002; Goldhirsch and Goldenberg, 2002; Kruyt, 2003; Luding et al., 2003; Madadi et al., 2004; Luding, 2004) and the references therein.

Recent research already addresses micro-macro transitions and micro-mechanics of granular media as well as the continuum description of those, including micro-polar theories where the rotational degree of freedom is important (Bardet and Vardoulakis, 2001; Suiker et al., 2001; Kruyt, 2003). The present work adds to this a new formulation based on the virtual displacement ansatz for single contacts. The method is not new, but the modular formulation provides a general formalism that can easily be extended to higher dimensions and involves also the tangential-forces and contact-moments (not shown here), which is expected to be helpful in the future. Many of the various approaches in the literature can be formulated as special cases of the formalism presented below. The numerical method of discrete element simulations alone is neither new nor original, see e.g. (Oda and Iwashita, 2000; Thornton, 2000; Lätzel et al., 2000) and the referencs therein, but the combination and quantitative comparison of numerical simulation with theoretical predictions is an issue rarely realized in the literature yet.

The new findings involve (i) an interesting qualitative difference in fabric- and stiffness-tensor component behavior under shear, (ii) an astonishing lack of sensitivity of the relation between fabric and coordination number to the addition of friction to the simulation model as compared to a non-frictional model (Madadi et al., 2004), and (iii) the observation that only three entries to the stiffness tensor are independent – for the system examined in its eigen-system. The latter issue concerns the anisotropy of the packing and the issue of anisotropic continuum theories, which is also rarely adressed in the framework of granular flows. In this study, the anisotropic material tensor is computed from a discrete particle simulation of a biaxial box set-up, and presented in average over many particles inside the system, far away from the walls; a study with space resolution that would unravel inhomogeneities like shearbands is in progress (Luding, 2004).

2 Micro-macro transition for one contact

In this section, the contact force law is reformulated in terms of contact stress, deformation, and stiffness – for single contacts. This leads to basic tensorial quantities associated with single contacts over which averages can be taken in a variety of ways. The single-contact stresses, e.g., do not constitute a macroscopic stress yet, but they are at the very basis of the micro-macro transition, and can be directly related to the "microscopic" force-displacement laws. Some of the possible averages are discussed, but by far not all of the possibilites can be considered in one paper. As final remark, it should be mentioned that this formulation is easily generalized to three dimensions, also for more complicated force-laws.

The vector connecting the centers of mass $\boldsymbol{r}_1$ and $\boldsymbol{r}_2$ of two particles, with radius a, is the so-called branch vector $\boldsymbol{l} = \boldsymbol{r}_1 - \boldsymbol{r}_2$, with the zero-force (contact) distance $l = |\boldsymbol{l}| = 2a$ and the corresponding unit vector $\hat{\boldsymbol{n}} = \boldsymbol{l}/l$, see also subsection 4.2. The overlap in normal direction $\boldsymbol{\Delta} = \boldsymbol{l} - 2a\hat{\boldsymbol{n}} =: \boldsymbol{\epsilon}^n \cdot \boldsymbol{l}$, is the deformation relative to the configuration when the particles just touch each other. This defines a tensor of rank two, $\boldsymbol{\epsilon}^n = \hat{\boldsymbol{n}}(\hat{\boldsymbol{n}} \cdot \boldsymbol{\epsilon})$, [1] which is the normal contribution of the deformation $\boldsymbol{\epsilon} = \boldsymbol{\epsilon}^n + \boldsymbol{\epsilon}^t$, relative to a virtual, stress-free reference configuration. With other words, $\boldsymbol{\epsilon}$ is the state variable conjugate to the stress – at least for the linear force model discussed here – such that $\boldsymbol{\sigma}^T : \boldsymbol{\epsilon}^{\mathrm{sym}} = \sigma_{\beta\alpha}\epsilon_{\alpha\beta}^{\mathrm{sym}} = u$, with the energy density u, see Eq. (5), the (transposed) stress σ, see Eq. (7), and the symmetric (objective) $\boldsymbol{\epsilon}^{\mathrm{sym}} = (1/2)(\boldsymbol{\epsilon} + \boldsymbol{\epsilon}^T)$. [2] The displacement in tangential direction $\boldsymbol{\vartheta} =: \boldsymbol{\epsilon}^t \cdot \boldsymbol{l}$, (also relative to a stress-free configuration) is irrelevant for perfectly smooth particles, but has to be taken into account for rough surfaces. This defines $\boldsymbol{\epsilon}^t = \hat{\boldsymbol{t}}^0(\hat{\boldsymbol{t}}^0 \cdot \boldsymbol{\epsilon})$, the tangential contribution to

$$\boldsymbol{\epsilon} = \frac{\Delta}{l}\hat{\boldsymbol{n}}\hat{\boldsymbol{n}} + \frac{\vartheta}{l}\hat{\boldsymbol{t}}^0\hat{\boldsymbol{n}} \, , \tag{1}$$

with $\hat{\boldsymbol{t}}^0 := \boldsymbol{\vartheta}/|\boldsymbol{\vartheta}|$. Note that $\boldsymbol{\epsilon}$ defines the deformation relative to the stress-

---

[1] The dot corresponds to a inner (scalar) tensor product that leads to a reduction of the rank by two, and no point corresponds to the outer (dyadic) product which leads to a tensor of rank equal to the sum of the two neighboring tensors.

[2] The deformation tensors $\boldsymbol{\epsilon}$ and $\boldsymbol{\varepsilon}$ can be non-symmetric, corresponding to a rotation of the contacting particles; from the non-symmetric deformation tensor, the non-objective contribution due to a rotation of the continuum has to be disregarded for objectivity reasons, so that the objective contributions remain [see the contribution by Jenkins and La Ragione in this issue]. The mean rotation of two particles can be formulated as an objective non-symmetric deformation in tangential direction, however, this will not be discussed further here.

free configuration such that $\boldsymbol{\epsilon} \cdot \boldsymbol{l} = \boldsymbol{\Delta} + \boldsymbol{\vartheta}$, and thus is not necessarily small, since overlaps and tangential displacements are not restricted a-priori. In contrast, a virtual, small (infinitesimal) change of the deformation is

$$\delta\boldsymbol{l} = \boldsymbol{l}' - \boldsymbol{l} =: \boldsymbol{\varepsilon} \cdot \boldsymbol{l} \approx \delta\boldsymbol{\Delta} + \delta\boldsymbol{\vartheta} = \delta\Delta\hat{\boldsymbol{n}} + \delta\vartheta\hat{\boldsymbol{t}} \ , \tag{2}$$

where the prime denotes the value after the deformation tensor $\boldsymbol{\varepsilon}$ is applied. Note that (especially in 3D), the vectors $\hat{\boldsymbol{t}}$ and $\hat{\boldsymbol{t}}^0$ are not necessarily parallel.

2.1 Change of the branch vector

When the packing of particles is deformed, it is most intuitive that the branch vector changes. This change, $\delta\boldsymbol{l}$, can be split in two components, one parallel to $\hat{\boldsymbol{n}}$, the other one perpendicular to it. The components of the normal change of $\boldsymbol{l}$ are $\delta\boldsymbol{\Delta} := \delta\boldsymbol{l}^n = \hat{\boldsymbol{n}}(\hat{\boldsymbol{n}} \cdot \boldsymbol{\varepsilon} \cdot \boldsymbol{l})$ and, expressed in index notation [3], read

$$\delta\Delta_\alpha = \delta l_\alpha^n = n_\alpha n_\beta \varepsilon_{\beta\gamma} l_\gamma \ . \tag{3}$$

The tangential components are $\delta\boldsymbol{\vartheta} := \delta\boldsymbol{l} - \delta\boldsymbol{l}^n$, or

$$\delta\vartheta_\alpha = \delta l_\alpha^t = t_\alpha t_\beta \varepsilon_{\beta\gamma} l_\gamma \ , \tag{4}$$

with the intrinsic definition of the tensor $t_\alpha t_\beta$ perpendicular to $n_\alpha n_\beta$. The tensor $n_\alpha n_\beta$ is a degenerate, one-dimensional tensor with eigen-direction parallel to $\hat{\boldsymbol{n}}$ and trace unity. In two dimensions $\hat{\boldsymbol{t}}$ defines the tangential direction modulo the sign. In both two and three dimensions, one can use $\hat{\boldsymbol{t}} := \delta\boldsymbol{l}^t/|\delta\boldsymbol{l}^t|$ as definition if $|\delta\boldsymbol{l}^t| > 0$. In three dimensions, this allows the definition of a third degenerate tensor perpendicular to both $\hat{\boldsymbol{n}}$ and $\hat{\boldsymbol{t}}$ via $s_\alpha s_\beta := 1_{\alpha\beta} - n_\alpha n_\beta - t_\alpha t_\beta$, with the unit-tensor denoted by the Kronecker-delta $1_{\alpha\beta}$.

2.2 Change of the potential energy density

The potential energy density for one contact,

$$u := u_c = \frac{1}{2V_c}\left(k\Delta^2 + k^t\vartheta^2\right) \ , \tag{5}$$

also changes due to a deformation, where k and k^t are the spring stiffness in normal and tangential direction, respectively (the prefactor of the quadratic

---
[3] Summation over equal indices is implied

4

term in a series expansion of the interaction potential), and the volume V_c will be specified later, since it can depend on the configuration of the particles in the neighborhood. Note that it is easy to specify the volume in any way (volume per contact, volume per contact of this particle, or volume associated to this contact via, e.g., a Voronoi tesselation or dual lattice construction, as used by Bagi (1996); Kruyt and Rothenburg (2001)), however, we prefer to leave it unspecified in order to keep a general formulation and since this volume disappears during averaging, in many cases.

Due to the displacement of one pair of particles, the change in potential energy density is

$$\delta u = \delta u^n + \delta u^t \approx \frac{1}{V_c} \left(k \Delta \delta l^n + k^t \vartheta_\alpha \delta_\alpha l^t \right) \approx \frac{1}{V_c} \boldsymbol{f}^* \cdot \boldsymbol{\varepsilon} \cdot \boldsymbol{l} \; , \tag{6}$$

with the actual force $\boldsymbol{f} = k \boldsymbol{\Delta} + k^t \boldsymbol{\vartheta}$, the force after displacement $\boldsymbol{f}' = \boldsymbol{f} + \delta \boldsymbol{f}$, and the mean $\boldsymbol{f}^* = (\boldsymbol{f} + \boldsymbol{f}')/2$. (The asterisk is dropped in the following for the sake of simplicity implying: $\boldsymbol{f} \approx \boldsymbol{f}^*$). Note the nice symmetry of the problem with respect to an exchange of the present configuration (unprimed) and the deformed configuration (primed).

2.3   The stress tensor

From the potential energy density, we obtain the transposed stress from the response to a virtual deformation by differentiation of u with respect to the deformation tensor components

$$\sigma_{\beta\alpha} = \frac{\partial u}{\partial \varepsilon_{\alpha\beta}} = \frac{1}{V_c} f_\alpha l_\beta \; . \tag{7}$$

For the result in Eq. (7), in symbolic notation: $\boldsymbol{\sigma} = (1/V_c) \boldsymbol{l} \boldsymbol{f}$, the partial derivative of the changes of the displacement vector with respect to the deformation tensor was replaced by the branch vector component and the identity tensors $1_{\alpha a} 1_{\beta b}$; the higher order terms in Eq. (6) were neglected.

Since both $\boldsymbol{l}$ and $\boldsymbol{\Delta}$ are parallel to $\hat{\boldsymbol{n}}$ and $\boldsymbol{\vartheta}$ is parallel to $\hat{\boldsymbol{t}}^0$, one can rewrite the stress tensor

$$\sigma_{\alpha\beta} = \frac{kl\Delta}{V_c} n_\alpha n_\beta + \frac{k^t l \vartheta}{V_c} n_\alpha t_\beta^0 \; , \tag{8}$$

and the stress increment tensor

$$\delta\sigma_{\alpha\beta} \approx \frac{kl\,\delta\Delta}{V_c} n_\alpha n_\beta + \frac{k^t l\,\delta\vartheta}{V_c} n_\alpha t_\beta \ , \tag{9}$$

with $\Delta = |\mathbf{\Delta}|$, $\delta\Delta = |\delta\mathbf{\Delta}|$, $\vartheta = |\boldsymbol{\vartheta}|$, and $\delta\vartheta = |\delta\boldsymbol{\vartheta}|$. Note that the dyadic product of the normal vectors $n_\alpha n_\beta$ is symmetric (and degenerate one-dimensional) by definition, whereas $n_\alpha t_\beta^0$ and $n_\alpha t_\beta$ are typically non-symmetric and traceless. The stress relations above are similar to those obtained earlier in the literature for many particle contacts (Bardet and Vardoulakis, 2001; Lätzel et al., 2000; Rothenburg and Selvadurai, 1981; Bathurst and Rothenburg, 1988; Bardet and Proubet, 1991; Bagi, 1996; Liao and Chang, 1997; Kruyt and Rothenburg, 1998, 2001; Ball and Blumenfeld, 2002; Kruyt, 2003).

2.4 The stiffness tensor

The partial derivative of the stress tensor with respect to the deformation leads to the stiffness tensor

$$C_{\alpha\beta\gamma\phi} = \frac{\partial\sigma_{\alpha\beta}}{\partial\varepsilon_{\phi\gamma}} = \frac{l^2}{V_c}\left(k\,n_\alpha n_\beta n_\gamma n_\phi + k^t n_\alpha t_\beta n_\gamma t_\phi\right) \ , \tag{10}$$

where the changes of the deformation in normal and tangential direction were used. The additional derivative which should occur in Eq. (10) leads to terms proportional to Δ/l, which are neglected in the following, since the overlap is typically much smaller than the distance between the particle centers.

Note that the stiffness tensor in Eq. (10) is similar to the results in the literature, see e.g. (Liao and Chang, 1997; Kruyt and Rothenburg, 1998), but here, particle-center to contact vectors are used instead of the frequently used particle-particle branch vector, and the stiffness contribution of a single contact only is given. In the next section, the relations are provided for particles inside larger averaging volumes.

3 Volume averaging

The purpose of this section is to present averages over the single-contact tensors from the previous section, for the sake of completeness, so that they can be compared to the previous literature, see e.g. (Rothenburg and Selvadurai, 1981; Liao and Chang, 1997; Kruyt and Rothenburg, 1998; Lätzel et al., 2000). The focus of the results presented in the next section is the fabric- and the stiffness-tensor, which can be obtained from static snapshots and do not rely on small (virtual or real) displacements.

6

Given the tensor-elements based on single contacts, one possibility is to compute the tensor for one particle in average over all its contacts. An alternative is to perform averages over all contacts within an averaging volume V, which is typically larger than one particle and thus can contain many contacts. As next refinement, each contact information can be "smeared out" via an averaging shape function, so that a fraction of it contributes to the averaging volume and the rest does not. Since we did not observe differences [4] using either of these methods together with the rather large V used below, the issue of averaging shape functions will not be discussed further here (Babić, 1997; Lätzel et al., 2000; Goldenberg and Goldhirsch, 2002; Goldhirsch and Goldenberg, 2002).

For the sake of simplicity, the simplest averaging approach is used here, i.e. a contact is taken into account if the corresponding particle center lies within the averaging volume. This corresponds to a pre-averaging over single particles and then subsequent averaging over the particles in the volume. Cast into an equation this reads

$$Q = \langle Q \rangle = \frac{1}{V} \sum_{p \in V} V^p Q^p \ , \tag{11}$$

where Q is the quantity to be averaged and $Q^p = (1/V^p) \sum_{c=1}^{C^p} V_c Q^c$ is the pre-averaged particle quantity with the contact quantity Q^c. Here, the sub-script $p \in V$ denotes the particle-in-volume averaging procedure; the equation for contact-in-volume averaging would appear as $Q = \frac{1}{V} \sum_{c \in V} V_c Q^c$. The volume fraction ν is obtained from either $Q^p = 1$, or from $Q^c = V^p/(C^p V_c)$, to name two examples. In the following, we restrict ourselves to the particle-in-volume averaging method.

3.1 The Fabric Tensor

For one particle, the fabric tensor is defined as the sum, over all contacts, of the dyadic product formed by the normal vectors:

$$F_{\alpha\beta}^p = \sum_{c=1}^{C^p} n_\alpha n_\beta \ , \tag{12}$$

with the trace $\mathrm{tr}\boldsymbol{F}^p = F_{\gamma\gamma}^p = C^p$. For one unit-cell (attributed to the single particle under consideration) with volume V^u, the fabric tensor can be defined

---

[4] For a centered averaging volume of about one third of the total volume, the particle-center in volume and the contact in volume averaging rules, respectively, slightly under- and overestimate the values obtained with a homogeneous shape function covering one particle, by less than one per-cent.

as

$$F_{\alpha\beta}^{u} = \frac{V^p}{V^u} \sum_{c=1}^{C^p} n_\alpha n_\beta \ . \tag{13}$$

so that $\mathrm{tr}\boldsymbol{F}^{u} = F_{\gamma\gamma}^{u} = \nu^u C^p$ is a contact number density with the (local) volume fraction $\nu^u = V^p/V^u$ and the contact number C^p of particle p. In a larger, disordered system, with some distribution of particle radii, the relation between fabric, density and contact number is more complicated (Madadi et al., 2004) and an average over many particles

$$F_{\alpha\beta} = \frac{1}{V} \sum_{p \in V} V^p \sum_{c=1}^{C} n_\alpha n_\beta \tag{14}$$

is the method of choice. Note that the super-script u for unit-cell is redundant, since the equations are identical to those with arbitrary averaging volume when the sum over the particles reduces to one term. The prediction for the trace of the fabric in frictionless, isotropic systems is

$$\mathrm{tr}\boldsymbol{F} = F_{\gamma\gamma} = g_2 \nu C \ , \tag{15}$$

with the average coordination number C, and the correction factor

$$g_2 \approx 1 + \frac{\sqrt{3}}{\pi} \left(\frac{\overline{a^3}}{\overline{a}\,\overline{a^2}} - 1 \right) \ , \tag{16}$$

dependent on the first three moments of the size distribution $\overline{a^k}$ (with $k = 1, 2, 3$), see the study by Madadi et al. (2004). In brief, g_2 corrects for the fact that the coordination number of different sized particles is proportional to their surface area, so that a monodisperse packing has $g_2 = 1$, whereas a polydisperse packing has $g_2 > 1$ with magnitude increasing with the width of the size distribution. Thus, a polydisperse packing has a higher contact number density than a monodisperse system of comparable density. Below, it will be shown that this correction, as tested for frictionless systems (Madadi et al., 2004), is also relevant for frictional packings.

8

In the averaging volume V, one obtains the approximate (averaged) macroscopic stress from Eqs. (8) and (11) so that:

$$\sigma_{\alpha\beta} = \frac{1}{V} \sum_{p \in V} \sum_{c=1}^{C} l_\alpha^c f_\beta^c \, , \tag{17}$$

where the particle volumes (and the arbitrary averaging volumes introduced for the single-particle relations) cancel due to the volume weight in Eq. (11).

3.3   The stiffness tensor

The stiffness tensor for spherical (disk) particles with branch vectors from the center to the contact $l^c = a$, and identical spring constants $k = k^c$ and $k^t = (k^t)^c$, is equivalently:

$$C_{\alpha\beta\gamma\phi} = \frac{1}{V} \sum_{p \in V} a^2 \left(k \sum_{c=1}^{C} n_\alpha^c n_\beta^c n_\gamma^c n_\phi^c + k^t \sum_{c=1}^{C} n_\alpha^c t_\beta^c n_\gamma^c t_\phi^c \right) \, , \tag{18}$$

where the two contributions from normal and tangential springs will be examined separately below. Again this result can already be found in the literature (Liao and Chang, 1997; Kruyt and Rothenburg, 1998) in similar form, however, we provide it here again, for the sake of completeness, in our nomenclature. More details and results on periodic lattices will be presented in a forthcoming paper (Luding, 2004).

4   Simulation Results

4.1   Model System

The discrete element model (DEM) (Herrmann et al., 1998; Vermeer et al., 2001; Cundall and Strack, 1979; Bashir and Goddard, 1991; van Baars, 1996; Oda and Iwashita, 2000; Thornton, 2000; Thornton and Antony, 2000; Oda and Iwashita, 2000; Kruyt and Rothenburg, 2001) is briefly introduced in this section, together with the force laws used in the simulation. The "experiment" chosen is the biaxial box set-up, see Fig. 1, where the left and bottom walls are fixed, and stress- or strain-controlled deformation is applied. In the first

case a wall is subject to a pre-defined pressure, in the second case, the wall is subject to a pre-defined strain. In a typical "experiment", the top wall is strain controlled and slowly shifted downwards, while the right wall moves stress controlled, dependent on the force $F(t)$ exerted on it by the material in the box. The strain-controlled position of the top wall as function of time t is here

$$z(t) = z_\text{f} + \frac{z_0 - z_\text{f}}{2}(1 + \cos \omega t) , \quad \text{with} \quad \varepsilon_\text{zz} = 1 - \frac{z}{z_0} , \tag{19}$$

where the initial and the final positions z_0 and z_f can be specified together with the rate of deformation $\omega = 2\pi f$. Rather large deformations $\varepsilon_\text{zz} \approx 0.10$ will be applied below. The cosine function is chosen in order to allow for a smooth start-up and finish of the motion so that shocks and inertia effects are reduced, however, the shape of the function is arbitrary as long as it is smooth and the deformation is slow.
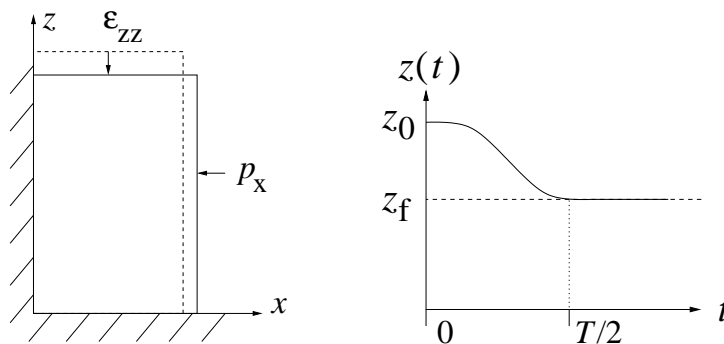

Fig. 1. (Left) Schematic drawing of the model system. (Right) Position of the top-wall as function of time for the strain-controlled situation.

The stress-controlled motion of the side-wall is described by

$$m_\text{w}\ddot{x}(t) = F(t) - pz(t) - \gamma_\text{w}\dot{x}(t) , \tag{20}$$

where m_w is the mass of the right side wall. Large values of m_w lead to slow adaption, small values allow for a rapid adaption to the actual situation. Three forces are active: (i) the force $F(t)$ due to the bulk material, (ii) the force $-p\,z(t)$ due to the external pressure, and (iii) a viscous frictional force, which damps the motion of the wall so that oscillations are reduced.

4.2 Discrete Particle Model

The elementary units of granular materials are mesoscopic grains which deform under stress. Since the realistic modeling of the deformations of the particles is

10

much too complicated, we relate the normal interaction force to the overlap Δ of two particles, see Fig. 2. Note that the evaluation of the inter-particle forces based on the overlap may not be sufficient to account for the inhomogeneous stress distribution inside the particles. Consequently, our results presented below are of the same quality as the simple assumptions about the force-overlap relation.
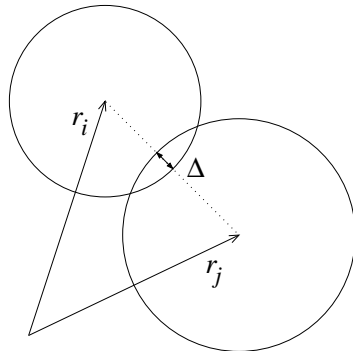

Fig. 2. (Left) Two particle contact with overlap Δ.

If all forces $\boldsymbol{f}_i$ acting on the particle i, either from other particles, from boundaries or from external forces, are known, the problem is reduced to the integration of Newton's equations of motion for the translational and rotational degrees of freedom

$$m_i \frac{\mathrm{d}^2}{\mathrm{d}t^2} \boldsymbol{r}_i = \boldsymbol{f}_i \ , \quad \text{and} \quad I_i \frac{\mathrm{d}^2}{\mathrm{d}t^2} \boldsymbol{\varphi}_i = \boldsymbol{t}_i \tag{21}$$

with the mass m_i of particle i, its position $\boldsymbol{r}_i$ the total force $\boldsymbol{f}_i = \sum_c \boldsymbol{f}_i^c$ acting on it due to contacts with other particles or with the walls, its moment of inertia I_i, its angular velocity $\boldsymbol{\omega}_i = \mathrm{d}\boldsymbol{\varphi}_i/\mathrm{d}t$ and the total torque $\boldsymbol{t}_i = \sum_c \boldsymbol{l}_i^c \times \boldsymbol{f}_i^c$.

4.2.1 Normal Contact Model

Two particles i and j interact only if they are in contact so that their overlap $\Delta := -\hat{\boldsymbol{n}} \cdot \boldsymbol{\Delta}$ is positive. The force on particle i, from particle j can be decomposed into a normal and a tangential part, where the simplest normal force is a linear spring and a linear dashpot

$$f_i^{\mathrm{n}} = k\Delta + \gamma_0 \dot{\Delta} \tag{22}$$

with spring constant k and some damping coefficient γ_0. The half-period of a vibration around the equilibrium position can be computed, and one obtains a typical response time $t_c = \pi/\omega$, with $\omega = \sqrt{(k/m_{ij}) - \eta_0^2}$, the eigenfrequency of the contact, the reduced mass $m_{ij} = m_i m_j/(m_i + m_j)$, and the rescaled

damping coefficient $\eta_0 = \gamma_0/(2m_{ij})$. The energy dissipation during a collision, as caused by the dashpot, leads to a restitution coefficient $r = -v'_n/v_n = \exp(-\eta_0 t_c)$, where the prime denotes the normal velocity after a collision.

4.2.2 Tangential Contact Model

The force in tangential direction is implemented in the spirit of Cundall and Strack (1979) who introduced a tangential spring in order to account for static friction. Various authors have used this idea and numerous variants were implemented, see (Brendel and Dippel, 1998) for a summary and discussion. Since we use a special implementation, which can be used for dimensions $D = 2$ and $D = 3$ alike, it is necessary to repeat the model and define the implementation. In the static case, the tangential force is coupled to the normal force via Coulombs law, i.e. $f^t \leq \mu^s f^n$, where for the sliding case one has the dynamic friction with $f^t = \mu^d f^n$. The dynamic and the static friction coefficients follow, in general, the relation $\mu^d \leq \mu^s$. However, for the following simulations we will apply $\mu = \mu^d = \mu^s$. The static case requires an elastic spring, related to $\boldsymbol{\vartheta}$ in section 2, in order to allow for a restoring force, i.e. a non-zero remaining tangential force in static equilibrium due to activated Coulomb friction.

If a contact exists with non-zero normal force, the tangential force is active too, and we project the tangential spring into the actual tangential plane [5]

$$\boldsymbol{\xi} = \boldsymbol{\xi}' - \boldsymbol{n}(\boldsymbol{n} \cdot \boldsymbol{\xi}') \; , \tag{23}$$

where $\boldsymbol{\xi}'$ is the old spring from the last iteration. This action is relevant only for an already existing spring; if the spring is new, the tangential spring-length is zero anyway, however, its change is well defined. The tangential velocity is

$$\boldsymbol{v}_t = \boldsymbol{v}_{ij} - \boldsymbol{n}(\boldsymbol{n} \cdot \boldsymbol{v}_{ij}) \; , \tag{24}$$

with the total relative velocity

$$\boldsymbol{v}_{ij} = \boldsymbol{v}_i - \boldsymbol{v}_j + a_i \boldsymbol{n} \times \boldsymbol{\omega}_i + a_j \boldsymbol{n} \times \boldsymbol{\omega}_j \; , \tag{25}$$

of the surfaces of the two contacting particles. Next, we calculate the tangential test-force as the sum of the tangential spring and a tangential viscous force (in analogy to the normal viscous force)

$$\boldsymbol{f}_o^t = -k_t \boldsymbol{\xi} - \gamma_t \boldsymbol{v}_t \; , \tag{26}$$

---

[5] This is necessary, since the frame of reference of the contact may have rotated since the last time-step

with the tangential spring stiffness k_t and a tangential dissipation parameter γ_t. As long as $|\boldsymbol{f}_o^t| \leq f_C^s$, with $f_C^s = \mu^s f^n$, one has static friction and, on the other hand, if $|\boldsymbol{f}_o^t|$ becomes larger than f_C^s, sliding, dynamic friction is active with $f_C^d = \mu^d f^n$. (In the next step, if $|\boldsymbol{f}_o^t|$ is smaller than f_C^s, static friction is active again, giving rise to stick-slip behavior.) In the former, *static* case, the tangential spring is incremented

$$\boldsymbol{\xi}' = \boldsymbol{\xi} + \boldsymbol{v}_t \,\delta t_{\mathrm{MD}} \ , \tag{27}$$

with the time step δt_{MD} of the DEM simulation. The new value of $\boldsymbol{\xi}'$ is to be used in the next iteration in Eq. (23), and the tangential force $\boldsymbol{f}^t = \boldsymbol{f}_o^t$ as defined in Eq. (26) is used. In the latter, *sliding* case, the tangential spring is adjusted to a length which is consistent with Coulombs condition

$$\boldsymbol{\xi}' = -\frac{1}{k_t} \left(f_C^d \, \boldsymbol{t} + \gamma_t \boldsymbol{v}_t \right) \ , \tag{28}$$

with the tangential unit vector, $\boldsymbol{t} = \boldsymbol{f}_o^t/|\boldsymbol{f}_o^t|$, defined by the direction of the force in Eq. (26), and thus the magnitude of the Coulomb force is used. Inserting $\boldsymbol{\xi}'$ into Eq. (26) leads to $\boldsymbol{f}_o^t \approx f_C^d \boldsymbol{t}$. Note that $\boldsymbol{f}_o^t$ and $\boldsymbol{v}_t$ are not necessarily parallel in three dimensions. However, the mapping in Eq. (28) works always, rotating the new spring such that the direction of the frictional force is unchanged and, at the same time, limiting the spring in length according to Coulombs law. In short notation the tangential force on particle i reads

$$\boldsymbol{f}_i^t = +\min \left(f_C, |\boldsymbol{f}_o^t| \right) \boldsymbol{t} \ , \tag{29}$$

where f_C follows the selection rules described above.

Note that the tangential force described above is identical to the classical Cundall-Strack spring only in the limits $\mu = \mu^s = \mu^d$ and $\gamma_t = 0$. The sequence of computations and the definitions and mappings into the tangential direction, however, is new to our knowledge in so far that it accounts for different static and dynamic friction coefficients and can be easily generalized to three dimensions.

4.2.3 Background Friction

Note that the viscous dissipation takes place in a two-particle contact. In the bulk material, where many particles are in contact with each other, dissipation is very inefficient due to long-wavelength cooperative modes of motion (Luding et al., 1994a,b). Therefore, an additional damping with the background is

13

introduced, so that the total force on particle i is

$$\boldsymbol{f}_i = \sum_c \left(f_i^n \hat{\boldsymbol{n}} + \boldsymbol{f}_i^t \right) - \gamma_{\mathrm{b}} \boldsymbol{v}_i \;,\tag{30}$$

with a viscous damping constant γ_{b} for a rapid equilibration.

4.2.4   Other Forces

Other forces than those mentioned above, like long-range forces, contact couples, rolling- or torsion-friction are neglegted in this study as well as a possible non-spherical shape of the particles. Research in this direction is in progress, however.

4.3   Parameters and initial configuration

The system examined in the following contains $N = 1950$ particles with radii a_i randomly drawn from a homogeneous distribution with minimum $a_{\mathrm{min}} = 0.5\,10^{-3}\,\mathrm{m}$ and maximum $a_{\mathrm{max}} = 1.5\,10^{-3}\,\mathrm{m}$. The masses of the cylindrical particles with height $h = 2.0\,10^{-4}\,\mathrm{m}$ are $m_i = \rho\pi h a_i^2$, with the density $\rho = 2.0\,10^3\mathrm{kg\,m^{-3}}$. The total mass of the particles in the system is thus $M \approx 0.0026\,\mathrm{kg}$ with the typical reduced mass of a pair of particles with mean radius, $m_{12} \approx 0.67\,10^{-6}\,\mathrm{kg}$. The wall properties are $m_{\mathrm{w}} = 10^{-4}\,\mathrm{kg}$ and $\gamma_{\mathrm{w}} = 2\,\mathrm{kg\,s^{-1}}$. If not explicitly mentioned, the material parameters are $k = 10^5\,\mathrm{N\,m^{-1}}$, $\gamma_0 = \gamma_t = 0.02\,\mathrm{kg\,s^{-1}}$, and $\gamma_{\mathrm{b}} = 10^{-5}\,\mathrm{kg\,s^{-1}}$, $\mu = 0.5$, and $k_t/k = 0.2$. This leads to a typical contact duration $t_c = 0.82\,10^{-5}\,\mathrm{s}$ and a restitution coefficient of $r = 0.89$, with the integration time-step used $\delta t_{MD} = 0.2\,10^{-6}\,\mathrm{s}$. The choice of parameters is rather arbitrary, however, the finding below that the stiffness tensor scales with the spring contstant rectifies this a-posteriori. Additional simulations (not shown here) also confirm this statement. Note that the choice of the stiffness and a possible non-linear force law is more important for dynamic systems for, e.g., sound propagation than for the quasi-static system presented here.

Initially, the particles are randomly distributed in a huge box, with rather low overall density. Then the box is compressed by allowing the walls to follow Eq. (20) with isotropic pressure $p = p_{\mathrm{x}} = p_{\mathrm{z}}$, in order to achieve an initial condition as isotropic as feasible; there is remainig anisotropy of the order of a few percent in some situations, however. This configuration is relaxed until the kinetic energy is several orders of magnitude smaller than the potential contact energy. Starting from the relaxed, isotropic initial configuration, the strain is applied to the top wall and the response of the system is examined, while the side wall is still pressure controlled. In Fig. 3, snapshots from a typical simulation are

14

shown during compression, displaying two important features. The potential energy (mean stress is equivalent to the potential energy density) increases together with the anisotropy (more vertical than horizontal stress-chains).
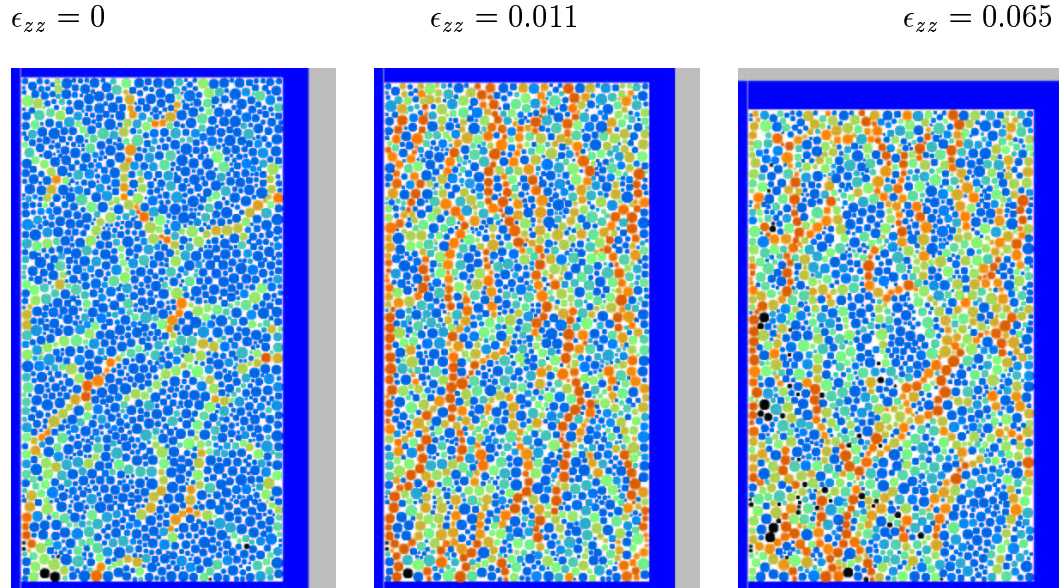
$\epsilon_{zz} = 0$ $\qquad\qquad\qquad\qquad\qquad \epsilon_{zz} = 0.011$ $\qquad\qquad\qquad\qquad\qquad \epsilon_{zz} = 0.065$

Fig. 3. Snapshots of the simulation at different ϵ_{zz}. The greyscale corresponds to the potential energy of each particle (summed over all its contacts), decaying from bright to dark.

4.4   Averaged Quantities

In the following, most simulation results are presented for the side pressure $p = 200$ only. A more detailed study involving various $p = 20, 40, 100, 200, 400$, and 500 is in preparation (Luding, 2004). There, the behavior of all the averaged scalar and tensor variables during the simulations is examined in detail for situations with low and high confining pressure. Here we focus on the fabric and the stiffness tensor.

The averages are performed such that parts of the system close to the walls are disregarded in order to avoid boundary effects. This means, that the averaging volume is only 64 per-cent of the total volume. A particle contact is taken into account for the average if the corresponding particle-center lies within the averaging volume V.

4.4.1   Fabric Tensor

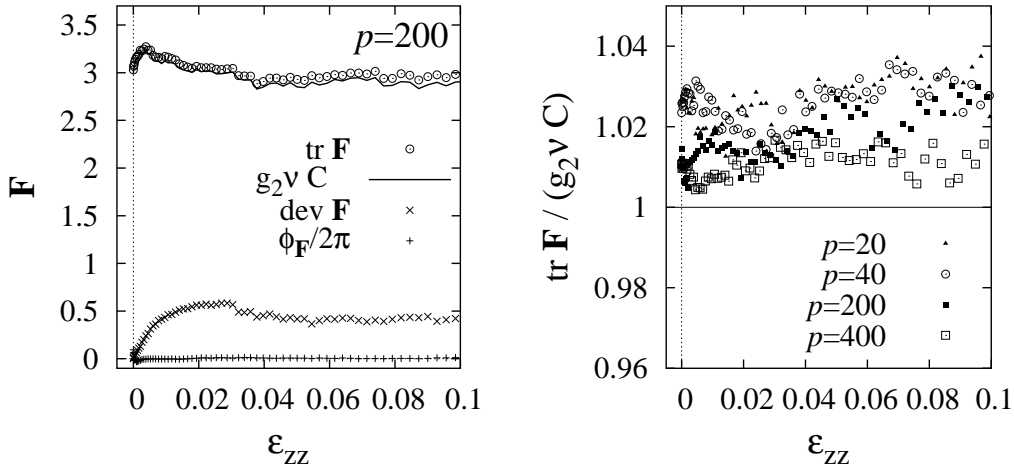The fabric tensor is computed according to Eq. (14), and displayed in Fig. 4.

15

Fig. 4. (Left) Fabric tensor, contact number density, deviator fabric, and fabric orientation ϕ_F, plotted against ε_{zz}. The contact number density is corrected by a factor $g_2 \approx 1.09$, which accounts for the polydisperse size-distribution (Madadi et al., 2004). (Right) Quality factor for the trace of the fabric tensor scaled by the analytical prediction $g_2 \nu C$ from (Madadi et al., 2004), for different pressures $p = 20$, 40, 200, and 400.

The trace of the fabric first (very rapidly) increases, due to the initial compression, and then decays at $\varepsilon_{zz} \approx 0.003$, due to the dilation; eventually, it reaches an almost stationary value for $\varepsilon_{zz} > 0.04$. This stationary contact number density is only slightly larger for higher pressure, and there is no strong difference for the deviator and the orientation as function of p. The former grows to values around 0.56 ± 0.03 until $\varepsilon_{zz} \approx 0.03$, and then decays to 0.40 ± 0.05. The latter remains close to zero, i.e. the mean fabric is almost always anisotropic during deformation, but not tilted away from the box geometry. The deviator grows to slightly smaller magnitude for larger confining pressure (data not shown here).

Note that the prediction for the trace was obtained from frictionless isotropic simulations. Given a correction of the order of eight to nine per-cent, the disagreement with our data of order one to two per-cent in the strongly anisotropic, frictional case indicates that the prediction by Madadi et al. (2004) is astonishingly robust. This shows that our definition of the fabric is promising with respect to its scaling behavior with ν and C. Nevertheless, the hidden secret is the functional behavior of C as function of the density and possibly other system- or material-parameters as well.

4.4.2   Stiffness tensor – normal contributions

The normal contributions of the stiffness tensor are plotted in Fig. 5, in units of k. The elements with an even number of one/two-indices (open symbols) are non-zero, whereas the entries with an odd number are always much smaller

16

(solid symbols). The difference of C^n_{1111} and C^n_{2222} indicates the anisotropy that is build up during the experiment, i.e. the material becomes stronger in vertical than in horizontal direction. Note that the vertical stiffness rapidly increases and remains at its saturation value from $\varepsilon_{zz} = 0.005$ to 0.03, whereas the horizontal stiffness decreases much slower and also does not saturate. For deformations larger than $\varepsilon_{zz} = 0.03$, vertical and horizontal stiffness decrease and increase, respectively, until they reach their large deformation limit. The variation of the shear stiffness C^n_{1122} is much less pronounced, but qualitatively follows the vertical stiffness. The small values of C^n_{1112} and C^n_{1222} (solid symbols) indicate that the eigen-system is not tilted much from the Cartesian and, expressed in terms of material behavior, means that the material does neither respond with a shear stress to a linear deformation nor with a linear stress to a shear deformation – in average [6]. As an interesting observation, we remark that the entry C^n_{1112} is larger in magnitude than C^n_{1222}. We relate this to the fact that the left and bottom wall of the simulation volume are fixed which breaks the symmetry of the problem and creates a preferred direction of tilt induced by the shear deformation and possibly related to (or caused by) the existence of a shearband.
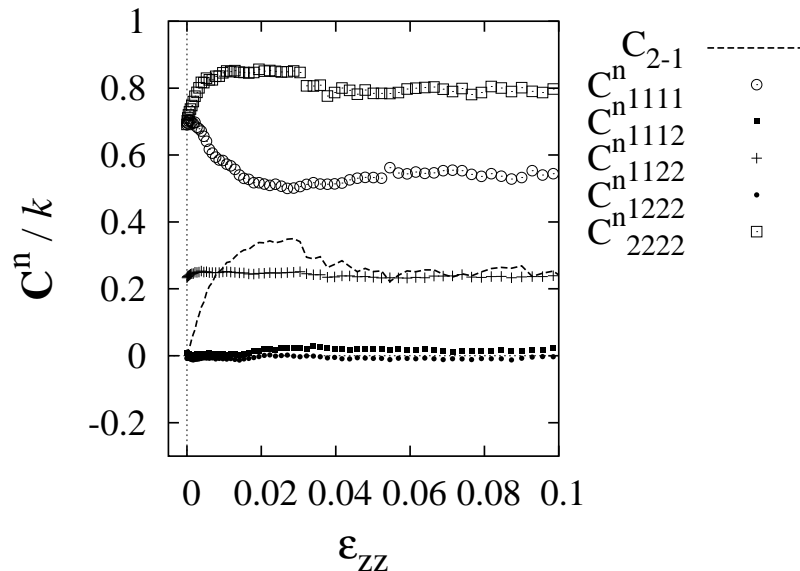

Fig. 5. Normal contributions to the material tensor $\boldsymbol{C}$. The dashed line is the difference between vertical and horizontal stiffness, $C_{2-1} = C^n_{2222} - C^n_{1111}$. The isotropically prepared initial configuration is in fact isotropic $C_{2-1} \approx 0$.
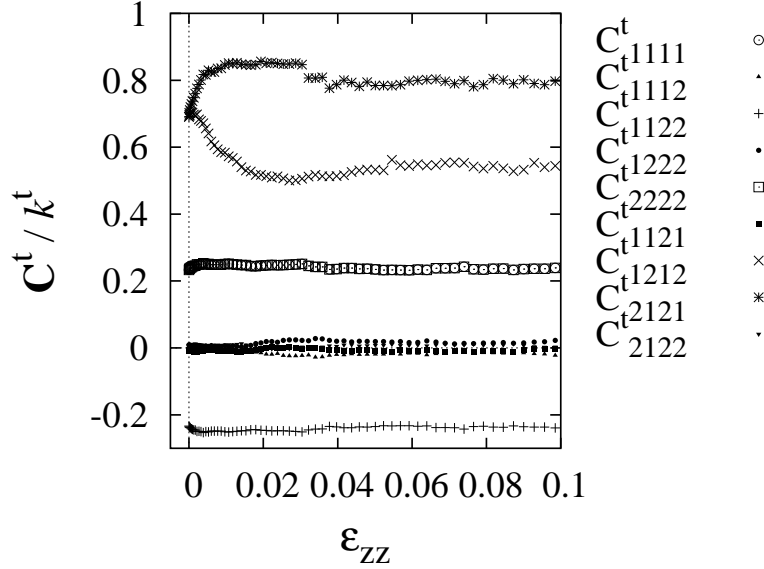
Fig. 6. Tangential contributions to the material tensor $\boldsymbol{C}$.

4.4.3 Stiffness tensor – tangential contributions

The tangential contributions $\boldsymbol{C}^t$ are plotted in Fig. 6, in units of k^t, where $\alpha = k^t/k^n$ is the ratio of tangential and normal stiffness. Note that $\alpha = 0.2$ as used for these simulations corresponds to a rather small overall contribution of the tangential forces to the global stiffness. The results are more complicated than for the normal contributions due to more different entries: The entries $C^t_{1111} = C^t_{2222} = \alpha C^n_{1122}$ (open symbols) are now identical and behave like the entry C^n_{1122}. In contrast, the entry $C^t_{1122} = -\alpha C^n_{1122}$ (plus symbol) interestingly has a negative sign. The entries C^t_{1112} and C^t_{1222} (dots) are again very small, and so are the new, possibly different entries C^t_{1121} and C^t_{2122} (small dots). The remaining two entries behave like the major entries in the normal tensor, i.e. $C^t_{1212} = \alpha C^n_{1111}$ and $C^t_{2121} = \alpha C^n_{2222}$ (x-symbol and star-symbol).

When the tiny entries of $\boldsymbol{C}$ are examined more closely, one observes that $\alpha C^n_{1112} = C^t_{1222}$ and $\alpha C^n_{1222} = C^t_{1121}$, while the entries $C^t_{1112} = -C^t_{1222}$ and $C^t_{2122} = -C^t_{1121}$ have the corresponding opposite sign.

4.4.4 Discussion of the anisotropy and its evolution

As could be expected from the experimental setup, the stiffness matrix behaves such that the material builds up strength against the direction of compression,

---

[6] If the deformation would not be parallel to the eigendirection of the anisotropy – as realized here in the bi-axial box set-up – such fully anisotropic behavior can be expected before critical state flow, until the contact network has adapted to the deformation.

and becomes weaker in the perpendicular direction. Both processes happen with different rate and different qualitative behavior – the vertical direction reaches its maximum rapidly and saturates, whereas the horizontal stiffness decreases slower. The tangential springs contribute less to the total stiffness than the normal springs, according to their smaller microscopic spring stiffness. The entry C_{1122}^t is interestingly negative, and the behavior of the normal stiffness tensor is reflected in the tangential stiffness tensor entries, however, in different ones. Finally, we note that the magnitude of the stiffness tensor entries is typically higher for larger external pressure (data not shown here), due to a larger contact number density.

Comparing the behavior of fabric and stiffness, one observes that the fabric trace, $\text{tr}\boldsymbol{F}$, remains almost constant, but the deviator, $F_D := \text{dev}\boldsymbol{F}/\text{tr}\boldsymbol{F}$, approaches a maximal value close to $F_D^{\max}(\nu, p)\text{tr}\boldsymbol{F} \approx 0.6$, a function of, at least, density and confining stress. The trace and the deviator, respectively, increase and decrease with the confining pressure. The anisotropy of the stiffness tensor, C_{1-2}, behaves similar to $\text{dev}\boldsymbol{F}$. Thus, answering the question what determines the empirical "yield-law": $F_D \le F_D^{\max}(\nu, p)$, will help to understand the evolution of anisotropy in granular packings based on geometric arguments. In relation to experimental observations, see section 5.2.3 in the paper by Calvetti et al. (1997), we propose the following differential equation, which describes the exponential approach of the deviatoric fabric to its limit value:

$$\frac{\partial F_D}{\partial \varepsilon_D} = \beta_F \left(F_D^{\max} - F_D \right) \ , \tag{31}$$

where $\beta_F = \beta_F(p)$ is a material parameter ($\beta_F(p = 200) \approx 82$), and the deviatoric deformation $\varepsilon_D = \varepsilon_{zz} - \varepsilon_{xx}$ is introduced. This equation is solved by

$$1 - \frac{F_D}{F_D^{\max}} = \exp\left(-\beta_F \varepsilon_D \right) \ , \tag{32}$$

in agreement with the simulation data for $\varepsilon_D \le 0.03$, with an error margin of about five per-cent. When the maximal anisotropy is reached, the behavior changes possibly due to shear band localization, and $F_D^{\max}$ is reduced to its critical state value F_D^{crit}.

Remarkable is here also that both $F_D^{\max}\text{tr}\boldsymbol{F}$ and $F_D^{\text{crit}}\text{tr}\boldsymbol{F}$ are only very weakly dependent on p. Note that $F_D \approx (F_{\max} - F_{\min})/(F_{\max} + F_{\min}) \approx (C_{2222} - C_{1111})/(C_{2222}+C_{1111}+2C_{1122})$, so that the above differential equation describes the fabric and the stiffness-anisotropy evolution as well.

Note that the formulation of a more general constitutive law for arbitrary

orientation of the deformation direction relative to the direction of the fabric eigen-values is far from the scope of this paper.

5   Conclusion

From the presented data, it can be concluded that there are basically only three different entries for the stiffness tensor, scaling with the microscopic spring stiffness used for the simulation. The normal contacts contribute the shear modulus and two (different) normal moduli. Besides the symmetry of the stiffness tensor with respect to all indices, another reason for this small number of quantities is the biaxial geometry that fixes the eigen-system of the tensorial quantities parallel to the walls. The stiffness tensor due to the tangential springs also scales with the corresponding spring stiffness and has also only three independent magnitudes (one entry being negative). This is interesting, because an anisotropic theory with only three stiffness parameters (plus the orientation of the eigen-system) is much easier to deal with than general anisotropic elasticity.

The second interesting finding is that friction has only a small effect on the scaling relation between fabric trace and the coordination number of the packing. However, this requires further investigation since the initial density was very high, and it cannot be excluded from the present data that a critical state flow with lower density and smaller coordination number is observed - however, this would contradict the critical state flow concept where, supposedly, the material has forgotton the initial state.

In the biaxial geometry we observe clear anisotropy of the fabric and the stiffness tensor. The magnitude of anisotropy is maximal at the point of maximum stiffness that coincides with the end of the dilatant regime with shear band localization (data not shown here, see Luding and Herrmann (2001); Luding et al. (2003)). The maximum of the fabric trace, interestingly, is found much earlier, closer to the onset of shear-banding. When the maximal anisotropy is reached eventually, the material becomes softer, until the measured quantities saturate in the critical flow regime. The scaled (dimensionless) anisotropy of the fabric and the stiffness tensor behave similarly, but the entries can behave qualitatively different.

A very simple constitutive relation for the evolution of the anisotropy (scaled deviatoric fabric and stiffness) with deviatoric deformation is proposed for the case of co-linear deformation and fabric. The limit deviator magnitude is approached exponentially fast. The microscopic and structural reasons for the limit in anisotropy is unclear as well as the detailed relation between stress, strain, and anisotropy. Future research involves a more detailed pa-

rameter study and three-dimensional simulations of similar systems. Since the data were obtained from averaging over the possibly inhomogeneous center of the system, ongoing research is directed towards a better resolution involving smaller averaging volumes in order to examine the effect of inhomogeneities on the conclusions above. The interesting finding, which supports the averaging used, is the fact that the eigen-direction of the averaged tensors remains (almost) parallel to the walls, whereas a tilt is expected inside the shear-band.

Acknowledgements

References

Babić, M. (1997). Average balance equations for granular materials. *Int. J. Engng. Sci.*, 35(5):523–548.

Bagi, K. (1996). Stress and strain in granular assemblies. *Mech. of Materials*, 22:165–177.

Bagi, K. (1999). Microstructural stress tensor of granular assemblies with volume forces. *J. Appl. Mech.*, 66:934–936.

Ball, R. C. and Blumenfeld, R. (2002). Stress field in granular systems: Loop forces and potential formulation. *Phys. Rev. Lett.*, 88:115505.

Bardet, J. P. and Proubet, J. (1991). A numerical investigation of the structure of persistent shear bands in granular media. *Géotechnique*, 41(4):599–613.

Bardet, J. P. and Vardoulakis, I. (2001). The asymmetry of stress in granular media. *Int. J. of Solids and Structures*, 38(2):353–367.

Bashir, Y. M. and Goddard, J. D. (1991). A novel simulation method for the quasi-static mechanics of granular assemblages. *J. Rheol.*, 35(5):849–885.

Bathurst, R. J. and Rothenburg, L. (1988). Micromechanical aspects of isotropic granular assemblies with linear contact interactions. *J. Appl. Mech.*, 55:17–23.

Brendel, L. and Dippel, S. (1998). Lasting contacts in molecular dynamics simulations. In Herrmann, H. J., Hovi, J.-P., and Luding, S., editors, *Physics of Dry Granular Media*, page 313, Dordrecht. Kluwer Academic Publishers.

Calvetti, F., Combe, G., and Lanier, J. (1997). Experimental micromechanical

analysis of a 2d granular material: relation between structure evolution and loading path. *Mech. Coh. Fric. Mat.*, 2:121–163.

Chang, C. S. and Ma, L. (1991). A micromechanical-based micropolar theory for deformation of granular solids. *Int. J. of Solids and Structures*, 21(1):67–86.

Cundall, P. A. and Strack, O. D. L. (1979). A discrete numerical model for granular assemblies. *Géotechnique*, 29(1):47–65.

Goldenberg, C. and Goldhirsch, I. (2002). Force chains, microelasticity, and macroelasticity. *Phys. Rev. Lett.*, 89(8):084302.

Goldhirsch, I. and Goldenberg, C. (2002). On the microscopic foundations of elasticity. *Eur. Phys. J. E*, 9(3):245–251.

Herrmann, H. J., Hovi, J.-P., and Luding, S., editors (1998). *Physics of dry granular media - NATO ASI Series E 350*, Dordrecht. Kluwer Academic Publishers.

Kishino, Y., editor (2001). *Powders & Grains 2001*, Rotterdam. Balkema.

Kruyt, N. P. (2003). Statics and kinematics of discrete cosserat-type granular materials. *Int. J. of Solids and Structures*, 40(3):511–534.

Kruyt, N. P. and Rothenburg, L. (1998). Statistical theories for the elastic moduli of two-dimensional assemblies of granular materials. *Int. J. of Engineering Science*, 36:1127–2242.

Kruyt, N. P. and Rothenburg, L. (2001). Statistics of the elastic behavior of granular materials. *Int. J. of Solids and Structures*, 38:4879–4899.

Lätzel, M., Luding, S., and Herrmann, H. J. (2000). Macroscopic material properties from quasi-static, microscopic simulations of a two-dimensional shear-cell. *Granular Matter*, 2(3):123–135. cond-mat/0003180.

Liao, C.-L. and Chang, T.-C. (1997). A generalized constitutive relation for a randomly packed particle assembly. *Computers and Geotechnics*, 20(3/4):345–363.

Luding, S. (2004). Micro-macro transition for anisotropic, periodic, elastic solids. in preparation.

Luding, S., Clément, E., Blumen, A., Rajchenbach, J., and Duran, J. (1994a). Anomalous energy dissipation in molecular dynamics simulations of grains: The "detachment effect". *Phys. Rev. E*, 50:4113.

Luding, S., Clément, E., Blumen, A., Rajchenbach, J., and Duran, J. (1994b). The onset of convection in molecular dynamics simulations of grains. *Phys. Rev. E*, 50:R1762.

Luding, S. and Herrmann, H. J. (2001). Micro-macro transition for cohesive granular media. in: Bericht Nr. II-7, Inst. für Mechanik, Universität Stuttgart, S. Diebels (Ed.).

Luding, S., Tykhoniuk, R., and Tomas, J. (2003). Anisotropic material behavior in dense, cohesive powders. *Chem. Eng. Technol.*, 26(12):1229–1232.

Madadi, M., Tsoungui, O., Lätzel, M., and Luding, S. (2004). On the fabric tensor of polydisperse granular media in 2d. *Int. J. Sol. Struct.*, 41(9-10):2563–2580.

Oda, M. and Iwashita, K. (2000). Study on couple stress and shear band

development in granular media based on numerical simulation analyses. *Int. J. of Enginering Science*, 38:1713–1740.

Peters, J. P. and Horner, D. A. (2002). Errors of scale in discrete element computations. In Cook, K. and Jensen, R. P., editors, *Discrete Element Methods: Numerical Modeling of Discontinua*, pages 56–67, Santa Fe. ASCE.

Rothenburg, L. and Selvadurai, A. P. S. (1981). A micromechanical definition of the Cauchy stress tensor for particulate media. In Selvadurai, A. P. S., editor, *Mechanics of Structured Media*, pages 469–486. Elsevier, Amsterdam.

Suiker, A. S. J., Metrikine, A. V., and de Borst, R. (2001). Comparions of wave propagation characterisitcs of the cosserat continuum model and corresponding discrete lattice models. *Int. J. of Solids and Structures*, 38:1563–1583.

Thornton, C. (2000). Numerical simulations of deviatoric shear deformation of granular media. *Géotechnique*, 50(1):43–53.

Thornton, C. and Antony, S. J. (2000). Quasi-static deformation of a soft particle system. *Powder Technology*, 109(1-3):179–191.

van Baars, S. (1996). *Discrete Element Analysis of Granular Materials*. PhD thesis, Technische Universiteit Delft, Delft, Nederlands.

Vermeer, P. A., Diebels, S., Ehlers, W., Herrmann, H. J., Luding, S., and Ramm, E., editors (2001). *Continuous and Discontinuous Modelling of Cohesive Frictional Materials*, Berlin. Springer. Lecture Notes in Physics 568.